

# Bayesian Convolutional Neural Networks for Limited Data Hyperspectral Remote Sensing Image Classification

Mohammad Joshaghani, Amirabbas Davari, Faezeh Nejati Hatamian, Andreas Maier, Christian Riess

**Abstract**—Employing deep neural networks for Hyper-spectral remote sensing (HSRS) image classification is a challenging task. HSRS images have high dimensionality and a large number of channels with substantial redundancy between channels. In addition, the training data for classifying HSRS images is limited and the amount of available training data is much smaller compared to other classification tasks. These factors complicate the training process of deep neural networks with many parameters and cause them to not perform well even compared to conventional models. Moreover, convolutional neural networks produce overconfident predictions, which is highly undesirable considering the aforementioned problem.

In this work, we use for HSRS image classification a special class of deep neural networks, namely a Bayesian neural network (BNN). To the extent of our knowledge, this is the first time that BNNs are used in HSRS image classification. BNNs inherently provide a measure for uncertainty. We perform extensive experiments on the Pavia Centre, Salinas, and Botswana datasets. We show that a BNN outperforms a standard convolutional neural network (CNN) and an off-the-shelf Random Forest (RF). Further experiments underline that the BNN is more stable and robust to model pruning, and that the uncertainty is higher for samples with higher expected prediction error.

**Index Terms**—Bayesian learning, convolutional neural networks, hyperspectral image classification

## I. INTRODUCTION

Hyperspectral remote sensing (HSRS) images serve many applications, ranging from urban planning, agricultural region monitoring, and natural resource management to material identification [1]. HSRS images are such a rich sources of information due to their dozens or hundreds of channels of different spectral wave-lengths [2]. On one hand, this high dimensionality demands a large number of training data. On the other hand, training data is typically expensive to acquire. These two factors and the fact that the training data does not scale with the data dimensionality result in the Hughes phenomenon [3]. This phenomenon challenges the training process of parametric machine learning methods, leading to over- and underfitting, inaccuracy, and convergence to non-optimal solutions.

This issue becomes more pressing with the increasing popularity of convolutional neural networks (CNNs) for classification tasks. CNNs reach outstanding performance on many computer vision tasks such as image classification. Deeper CNNs are capable of extracting more expressive features and

modeling more complex functions. However, the number of parameters scales with the depth of the network. Hence, limited training data easily cause the CNN to overfit.

In this work, we explore Bayesian neural networks (BNN) to alleviate this challenge. BNNs are a specific variant of deep neural networks. In BNNs, the network parameters of one or more layers are replaced by probability distributions. When performing network inference, a specific set of weights is sampled from these distributions. Hence, one can view a BNN as a distribution of networks. This distribution enables ensembling by performing multiple inference steps. Then, the prediction is the mean of the ensemble results, and their variance can serve as an additional uncertainty measure.

Ensembling is a well-known and effective tool to tackle overfitting, and we show in our experiments that BNNs indeed improve the overall classification performance. Additionally, the learned weight distributions of the BNN can provide valuable insights. We specifically use these weight distributions to prune the network by removing the least informative weights from the network.

In detail, our specific contributions are

- 1) We propose Bayesian Neural Networks for HSRS image classification on limited training data. We demonstrate its performance in comparison to a comparably constructed standard CNN and a classical random forest classifier. To our knowledge, this is the first time that BNNs are used for HSRS image classification.
- 2) We show two applications of the network. First, we demonstrate that the distributions of weights in the BNN can be effectively used to prune the network, which makes the BNN more compact and enables its use also on resource-limited devices. This pruning reduces the original parameter set by an order of magnitude with only small impact on classification performance. Second, we gradually omit test samples with high uncertainty to show that the samples with uncertainty are indeed more likely to be misclassified.

The rest of this paper is organized as follows: Section II reviews the related work. Section III briefly overviews the mathematical background of the Bayesian neural network. Section IV explains the proposed HSRS classification pipeline. In Sec. V, the experiments and their settings, as well as their results are discussed. Finally, Sec. VI concludes this work.

M. Joshaghani, A. Davari, F. Nejati Hatamian, A. Maier and C. Riess are with the Computer Science department at Friedrich-Alexander University Erlangen-Nürnberg, 91058 Erlangen, Germany (email: amir.davari@fau.de).

## II. RELATED WORKS

This section is organized in three parts. We first discuss works that address the issue of limited data in HSRS image classification. Then, we review convolutional neural networks for HSRS image classification. Third, we introduce prior work on Bayesian neural networks.

**Limited Training Data.** Several works have been conducted to tackle the issue of limited training data. As suggested by Davari *et al.* [4], the solutions can be classified in three classes: 1) Developing new architectures or adapt techniques in the current architectures, such as regularizers and data augmentation, to boost network's performance in this condition [6], [7], [8], 2) Reducing the dimensionality of the feature vectors to feed the classifiers more informative data, and 3) Artificially generating synthetic data to increasing the number of training data [4], [5], [9].

Since there is a large redundancy in spectral channels in HSRS images, applying dimensionality reduction techniques, such as PCA, is highly effective. In [10], to reduce the dimensionality of edge preserving filters, PCA is used. The dimensionality of the filters are reduced before feeding them to the classifier. The authors show that such feature vectors are powerful and provide performance improvement. Other works use PCA after the feature vector, e.g., extended multi-attribute profile (EMAP) [11], to provide a more powerful and informative feature vector to the model [4], [5]. Following them, we also adapt this approach and use PCA on EMAP features to improve the performance.

Although promising, synthetically populating severely small training data using generative models is limited. Several works use GANs [12] to generate the synthetic data to be added to the training pool [13], [14]. The main disadvantage of these methods is the fact that generative models such as GANs require a relatively high amount of training data in order to capture the underlying distribution of the data accurately.

**CNNs in HSRS image classification.** Deep CNN networks are dominant in many computer vision tasks, such as classification. Recently, CNNs also started to receive attention from researchers in HSRS image classification. They are reported to outperform established HSRS classification baselines. Additionally, it has been reported that using spatial and spectral features together will increase the classification accuracy [15], [16], which is one advantage of convolutional-based architectures used on HSRS images is they inherently use data across the channel as well.

Chen *et al.* [17] proposed stacked autoencoders (SAE) to learn abstract HSRS image features in an unsupervised fashion. The resulting feature set was then fed into a logistic regression for classification of HSRS images. In another work, the same authors proposed to replace SAE by a deep belief network (DBN). Considering the similarity of DBNs and CNNs, their work is one of the first ones that pioneered the use of deep neural network for HSRS image classification. Makantasis *et al.* [18] used a 2-D CNN architecture, and reduces the dimensionality of the data via PCA to three dimensions, trying to process it as RGB image data. However, some other works use 3-D CNN that work with raw data or

with dimensionality-reduced data [19], [20]. Audebert *et al.* provides a review article deep learning methods that are used in HSRS image classification [21].

It is a difficult task to perform CNN training for HSRS image classification with only very limited training data. Chen *et al.* [22] proposed to combine Gabor filters with convolutional filters, where the Gabor filters are used to encode spatial information like textures and edges. Other works explore various data augmentation algorithms to mitigate the limited training data size [23], [24]. A general strategy is to fine-tune a network that was pre-trained on a larger datasets like ImageNet. Eventhough the data for fine-tuning itself is insufficient, this training strategy generally improves the classification performance. He *et al.* [25] proposed transfer learning in combination with ensemble learning. They used a ImageNet-pretrained network and randomly selected three channels of the HSRS image to fine-tune multiple networks. Finally, they used the resulting networks in an ensemble learning scheme. Alternatively, active learning has been utilized to remedy the limited data problem. Cao *et al.* [26] proposed to iteratively train a CNN on a small training set. Then, they select the most informative pixels from a candidate pool, and fine-tune the network on the new training dataset.

**Bayesian neural networks.** Several studies have applied Bayesian methods to neural networks. The main challenge is that it is intractable to compute the true posterior probability distribution. Therefore, different approximation methods have been investigated and proposed to compute the posterior. Buntine and Weigend [27] proposed different maximum a-posteriori (MAP) schemes for neural network and considered second order derivatives in the prior probability approximation. Several other attempts have been made to improve the approximation quality while keeping the computation tractable and applicable on modern applications [28], [29]. However, two approaches are the most successful among them. The first one is to construct the Bayesian network using Dropout [30] and Gaussian Dropout [31] as approximate variational inference schemes [32]. The second approach builds the Bayesian neural network using Backprop [33], [28] based on variational inference. It considers Gaussian probability distribution over the weights, which are defined using two parameters, mean and variance [34]. Both approaches provide methods to approximate uncertainty. In [34], a comparison of the two approaches is made and they are shown to perform comparably on MNIST dataset [35]. As explained in [34], the Softplus normalization, applied to *Bayes by Backprop*-based variational inference to estimate uncertainties, is more appropriate to use in computer vision tasks.

To the extent of our knowledge, Bayesian neural networks have never been employed in this field. In this work, our focus is to employ them on HSRS image classification task. We perform extensive evaluation of the Bayesian model and compare different aspects of the model with a conventional (non-Bayesian) model.

## III. BAYESIAN CONVOLUTIONAL NEURAL NETWORK

Frequentist neural networks have a tendency to produce overconfident predictions. Besides, when not provided with

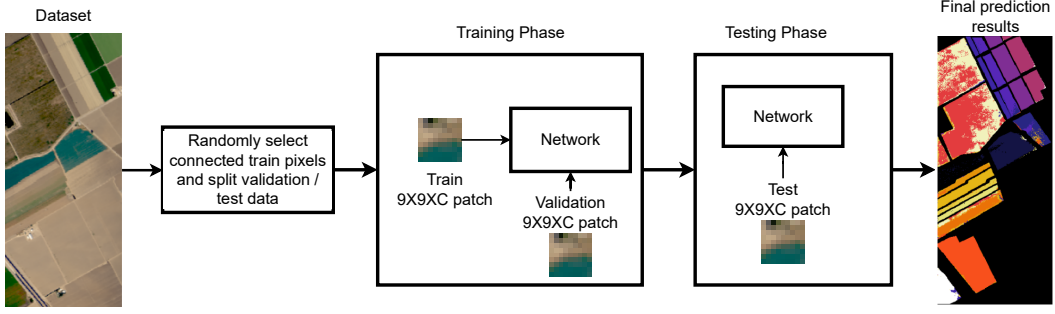


Fig. 1: HSRS image classification pipeline.

enough training data, they are prone to the overfitting problem. Combining the idea of Bayesian learning with standard neural networks can address these limitations. Bayesian models perform predictions by integrating over the distribution of possible models and the prior probability. This enables an intrinsic regularization making them more robust against overfitting.

The BNN in this work follows the work by Shridhar *et al.* [36]. It is a Bayesian Convolutional Neural network (BCNN) that uses Variational Inference. This section provides a brief background on the network. For a more in-depth discussion, the reader is referred to [36].

#### A. Variational Inference

Bayesian neural networks train a model by inferring the model posterior. Accurate inference of the model posterior is computationally demanding, and even for only moderately sized models intractable. Hence, the model posterior is usually approximated. One popular and successful approximation method is variational inference.

Given the input set  $\mathbf{X} = \mathbf{x}_1, \mathbf{x}_2, \dots, \mathbf{x}_N$  and a corresponding output set  $\mathbf{y} = y_1, y_2, \dots, y_N$ , then the functor  $f(\mathbf{X}) = y$  estimates the output  $y$  from the inputs  $\mathbf{X}$ . Bayesian learning provides a principled approach to obtain the model posterior  $p(f|\mathbf{X}, \mathbf{y})$ . Two components are required to calculate the posterior. First, a prior distribution  $p(f)$  that captures a prior belief about the estimator functions. Second, a likelihood function  $p(\mathbf{y}|f, \mathbf{X})$  for indicating how likely it is for the model  $f$  to predict the output  $y$  given the observations  $\mathbf{X}$ .

More specifically, given an unseen data  $(\mathbf{x}^*, y^*)$ , the posterior is obtained by integrating over all possible estimator functions  $f$  that are parametric models with parameter set  $\theta$ ,

$$\begin{aligned} p(y^*|\mathbf{x}^*, \mathbf{X}, \mathbf{y}) &= \int p(y^*|f)p(f|\mathbf{x}^*, \mathbf{X}, \mathbf{y})df \\ &= \int p(y^*|f)p(f|\mathbf{x}^*, \theta)p(\theta|\mathbf{X}, \mathbf{y})df d\theta . \end{aligned} \quad (1)$$

This integral is intractable due to the intractability of the distribution  $p(\theta|\mathbf{X}, \mathbf{y})$ . Hence, the variational approach is to approximate  $p(\theta|\mathbf{X}, \mathbf{y})$  with a variational distribution  $q(\theta)$ . The candidate  $q(\theta)$  should be as similar as possible to the original intractable distribution. The similarity of  $p(\theta|\mathbf{X}, \mathbf{y})$  and  $q(\theta)$  can be assessed with the Kullback-Leiber (KL) divergence [37]. Minimizing the mentioned KL divergence is equivalent to

maximizing the log evidence lower bound with respect to the parameter set  $\theta$

$$\text{KL}_{\text{VI}} = \int q(\theta)p(F|\mathbf{X}, \theta) \log_p(\mathbf{y}|F)dF d\theta - \text{KL}(q(\theta)||p(\theta)) . \quad (2)$$

Maximizing  $\text{KL}_{\text{VI}}$  results in a variational function that approximates the posterior. The approximation  $q(\theta)$  simplifies equation 1 to

$$q(y^*|\mathbf{x}^*) = \int p(y^*|f)p(f|\mathbf{x}^*, \theta)q(\theta)df d\theta . \quad (3)$$

When the network performs inference, the network parameters  $\theta$  are sampled from  $q(\theta)$ .

#### B. BNN Training via Back-Propagation

In *Bayes by Backprop* [28], [33], the posterior distribution on the neural network's weights is learned. Since the true posterior is often intractable, an approximate distribution  $q_\alpha(\theta)$  similar to the true distribution  $p(\theta)$  is defined. The training consists of minimizing the KL divergence of  $q_\alpha(\theta)$  and the true intractable posterior  $p(\theta)$  by finding the optimal parameter  $\alpha$ . This is done by approximating the integral from Eq. 2 with  $n$  drawn samples,

$$F(\mathcal{D}, \alpha) \approx \sum_{i=1}^n \log q_\alpha(\theta^{(i)}|\mathcal{D}) - \log p(\theta^{(i)}) - \log p(\mathcal{D}|\theta^{(i)}) , \quad (4)$$

where  $\mathcal{D}$  is the training dataset.  $\theta^{(i)}$  is a sample from the variational distribution  $q_\alpha(\theta|\mathcal{D})$ , which we set as a Gaussian distribution with mean and standard deviation as parameters. The cost function in Eq. 4 consists of three terms. First,  $\log q_\alpha(\theta^{(i)}|\mathcal{D})$  is the variational posterior with mean  $\mu$  and standard deviation  $\sigma$ ,

$$\log q_\alpha(\theta^{(i)}|\mathcal{D}) = \sum_i \log \mathcal{N}(\theta_i|\mu, \sigma^2) . \quad (5)$$

Second,  $\log p(\theta^{(i)})$  denotes the log prior, which is a zero-mean Gaussian distribution

$$\log p(\theta^{(i)}) = \sum_i \log \mathcal{N}(\theta_i|0, \sigma_p^2) . \quad (6)$$

Third, the likelihood  $\log p(\mathcal{D}|\theta^{(i)})$  is the network output.

### C. Bayesian Neural Network with Variational Inference

To fuse Bayesian learning in CNNs and tackle the intractable posterior distribution problem via variational inference, it is necessary to build convolutional layers with a probability distribution over the weights as filter weights, as well as fully-connected layers. In this case, the weights would be samples from the corresponding distribution. As mentioned in the previous section, the distributions are Gaussian, and each weight distribution is defined by its mean  $\mu$  and variance  $\sigma$ .

To adapt this idea on the convolutional layers, Shridhar *et al.* used Local Re-parameterization technique [38]. It is simply re-writing and re-parameterizing the equations above to translate the global uncertainty to the local uncertainty. Using this trick, instead of directly sampling the weights, the activation maps  $b$  are sampled, leading to more efficient and faster computational.

Consider the network weights variable  $\mathbf{w}$ . The variational posterior  $q_{\mathbf{w}}(\mathbf{w}_{ijhw}|\mathcal{D}) = \mathcal{N}(\mu_{ijhw}, \alpha\mu_{ijhw}^2)$ , where  $i$  and  $j$  are inputs, and  $h$  and  $w$  are filter height and width. This results in the following for the activation of convolutional layer for the corresponding receptive field  $R_i$ :

$$b_j = R_i * \mu_i + \epsilon_j \odot \sqrt{R_i^2 * (\alpha_i \odot \mu_i^2)} , \quad (7)$$

where  $\epsilon_j \sim \mathcal{N}(0, 1)$ ,  $\odot$  is the element-wise multiplication, and  $*$  is the convolution operator. As it can be observed, this trick transforms the convolutional operation within a layer into two operations: First, the output of  $b$  is treated as a frequentist output and gets updated by Adam optimizer. This single-point estimate is considered as the mean of the posterior. In the second operation, the variance of the distribution is learned. This formulation ensures a non-zero positive variance. Shridhar *et al.* introduced Softplus activation function to accommodate both operations [34].

### D. Softplus Activation Function

Two operations are applied in the convolutional and fully connected layers. One accounts for mean  $\mu$ , and the other accounts for the variance  $\alpha\mu^2$ . Applying Softplus [34] ensures a non-zero positive variance after the training. It is a smooth approximation of ReLU activation function, but it does not reach zero when the input approaches minus infinity. Softplus is defined as

$$\text{Softplus}(x) = \frac{1}{\beta} \log(1 + \exp(\beta x)) . \quad (8)$$

By default,  $\beta$  is set to 1.

### E. Uncertainty in Bayesian Neural Networks

One of the main advantages of Bayesian neural networks over frequentist neural networks is the ability to express uncertainty. Bayesian learning allows to distinguish two types of uncertainty, namely *aleatoric* and *epistemic* uncertainty [39]. *Aleatoric* uncertainty captures uncertainty caused by the data, e.g., inherent noise in data, whereas *epistemic* uncertainty captures the model uncertainty. For example, this implies that if the model is provided with more data from the same underlying

distribution, then the epistemic uncertainty will be reduced, but the aleatoric uncertainty will remain at the same level.

On real data, there is typically no closed-form solution for the predictive distribution. However, an unbiased estimator of the expected value of the predictive distribution can be written as

$$\mathbb{E}_q(p_{\mathcal{D}}(y^*|\mathbf{x}^*)) = \int q_{\alpha}(\mathbf{w}|\mathcal{D})p_{\mathbf{w}}(\mathbf{y}|\mathbf{X})d\mathbf{w} \quad (9)$$

$$\approx \frac{1}{T} \sum_{t=1}^T p_{\mathbf{w}_t}(y^*|\mathbf{x}^*) , \quad (10)$$

where  $T$  is the number of samples. The variance of this expected value can be decomposed into the aleatoric and epistemic uncertainty. More specifically, the *aleatoric* uncertainty is calculated as

$$\text{Aleatoric} = \frac{1}{T} \sum_{t=1}^T (\text{diag}(\hat{\mathbf{p}}_t)) - \hat{\mathbf{p}}_t \hat{\mathbf{p}}_t^T , \quad (11)$$

and the epistemic uncertainty is calculated as

$$\text{Epistemic} = \frac{1}{T} \sum_{t=1}^T (\hat{\mathbf{p}}_t - \bar{\mathbf{p}})(\hat{\mathbf{p}}_t - \bar{\mathbf{p}})^T , \quad (12)$$

where  $\hat{\mathbf{p}}_t$  denotes the network output, i.e.  $\text{Softmax}(f_{\mathbf{w}_t}(\mathbf{x}^*))$ , and  $\bar{\mathbf{p}}$  is the average of  $\hat{\mathbf{p}}_t$  over different samples, i.e.  $\frac{1}{T} \sum_{t=1}^T \hat{\mathbf{p}}_t$ . For a derivation of these equations, the reader is referred to [36].

## IV. BAYESIAN NEURAL NETWORK FOR HSRS IMAGE CLASSIFICATION

Figure 1 shows an overview of the classification pipeline. The data is split into training, validation, and test sets. Then, the model is trained on the training set, and after each epoch, the model is validated. After the training, the model with the best validation kappa score is selected and evaluated on the test set.

Deep neural networks are in principle capable of extracting the features from raw input data. However, quality and quantity of the training data are important requirements for training convergence to a good-performing feature extractor. When the limited data is scarce, the network may not converge. In such a case, they can benefit from a pre-processing step that eliminates redundancy and reduces the feature dimensionality. In this spirit, we calculate EMAP features and further reduce the feature vector via PCA analogously to previous works, e.g., Aptoula *et al.* [23].

We study three aspects to assess the benefits of Bayesian neural networks for the classification of limited-data HSRS images:

### A. Comparison of Classification Performance of BNN versus Standard CNN

We first investigate how the BNN performance compares to the performance of a standard CNN with identical architecture. Furthermore, the BNN can be considered as a distribution of networks from which a (theoretically infinite) number of networks can be sampled. Ensembling generally leads to

performance improvement and robustness against overfitting. Hence, we specifically add a comparison between the BNN before and after ensembling.

### B. Robustness Against Overfitting

Overfitting is one of the main challenges that severely limited training data imposes to the learning process. We monitor the evolution of the network performance on the training and validation sets. This provides an effective tool to identify the existence of overfitting. We compare the BNN and CNN side-by-side to show that the BNN is more robust against overfitting on limited training data.

### C. Model Pruning

The distribution of the weights may provide additional insights into the network quality. Performing the classification on a smaller sub-network may indicate that less network weights are involved in the largest contribution to the prediction performance. We investigate this behavior by iteratively pruning the model weights for both the BNN and CNN while observing their classification performance.

## V. EXPERIMENTAL RESULTS

### A. Dataset

In this work, we use the commonly used and publicly available Pavia Centre, Salinas, and Botswana datasets for evaluation. Figure 2 illustrates the class distribution of the datasets. Salinas dataset was acquired by the AVIRIS sensor over the Salinas Valley, California. There are  $512 \times 217$  samples in the dataset. It is comprised of 16 classes, including different types of vegetation, fields and soil.

Botswana dataset was acquired by NASA EO-1 satellite using the Hyperion sensor in 242 bands over the Okavango Delta, Botswana. After removing the noisy bands, the raw dataset has 145 spectral channels. This dataset comprises of 14 classes, including different swamps and woodlands. The number of available labeled pixels is 3248.

The Pavia Centre dataset has been acquired by the ROSIS sensor in 102 spectral bands over Pavia, northern Italy. The original scene is a  $1096 \times 1096$  image, however, some sections of the image contains no data and is blank. After removing that section, the resolution would be  $1096 \times 715$  pixels. This dataset contains 148152 labeled pixels in 9 classes. Compared with the other two datasets, this dataset has larger homogeneous regions.

### B. Experimental Setup

1) *Pre-processing*: Throughout all experiments, we use EMAP-PCA as feature descriptor [4], [5]. This descriptor first applies PCA to the raw hyperspectral image data. The eigenvectors that are associated with the largest eigenvalues preserve 99% of the total spectral variance, while greatly reducing redundancies between spectral bands. Then, extended multi-attribute profile (EMAP) features [11], [40] are computed. These features require four thresholds  $\lambda$  for the area of connected components, which we set as  $\lambda = [100, 500, 1000, 5000]$ . Finally, we use

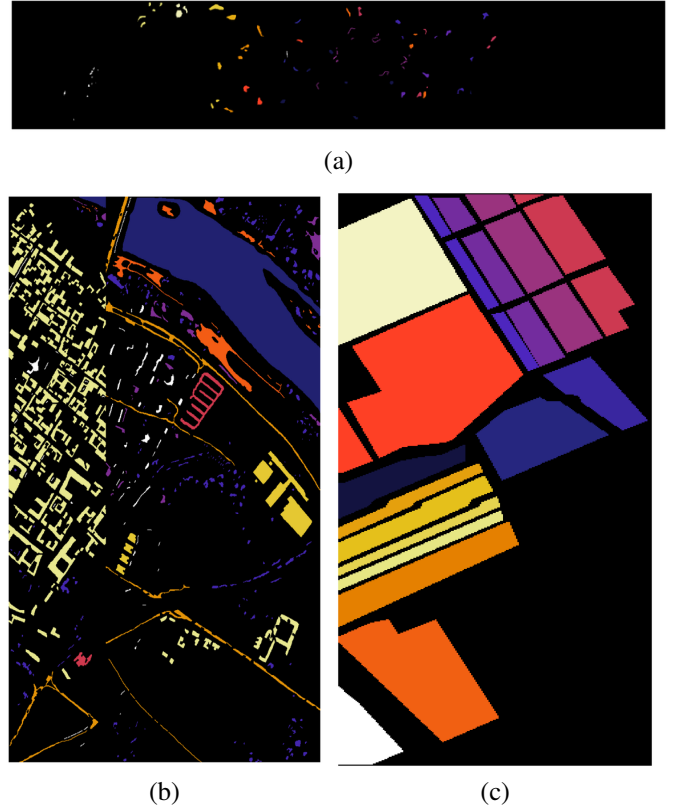


Fig. 2: (a) Botswana, (b) Pavia Centre, and (c) Salinas datasets ground truth classes.

PCA again to preserve 99% of the feature variance. Before feeding the data to the network, the feature vectors go through min-max normalization, which scales them between  $[0, 1]$ .

2) *Data Split*: In order to best evaluate the model performance, we split the data into train, validation, and test sets. The model is trained and then evaluated, and the model with the best evaluation scores is selected and again evaluated with the test set. The provided results are obtained from the test set.

We devoted particular attention to the composition of the training and test splits, in order to reduce avoidable correlations between training, validation, and test data. More in detail, the neural network filters operate on spatial regions of  $9 \times 9$  pixels centered at a pixel of interest. Hence, it is desirable that all pixels in this  $9 \times 9$  region belong to the same dataset (training, validation, test), to realistically assess the generalization performance. To this end, the training data pixels are not simply randomly drawn from the whole dataset. Instead, one pixel per class is drawn randomly, and only the connected component of pixels with the same class as the randomly drawn pixel is used as a basis for the training. More details on this approach are presented in the supplemental material.

3) *Experimental Setup and Hyperparameters*: The experimental comparison includes two baseline methods, namely a standard feed-forward CNN with a similar architecture to the proposed BNN, and an off-the-shelf Random Forest [41]. For brevity and disambiguation, we denote throughout our experiments the standard CNN as “CNN”, and the proposed



TABLE I: Network architecture details.

Block Name	input size	output size	kernel size	#filters
CNN block 1	$8 \times 8$	$7 \times 7$	$3 \times 3$	128
CNN block 2	$128 \times 7 \times 7$	$256 \times 5 \times 5$	$3 \times 3$	256
CNN block 3	$256 \times 5 \times 5$	$512 \times 3 \times 3$	$3 \times 3$	512
Flatten	$512 \times 3 \times 3$	4068		
Dense 1	4068	# labels		
Log Softmax	# labels	# labels		

Bayesian Convolutional Neural Network as “BNN”.

The loss function for training the standard CNN is the categorical cross-entropy. The loss function for training the BNN is the Variational Gaussian loss. The random forest objective function is the Gini index. The optimizer is set to Adam with initial learning rate of 0.001. Data augmentation is used to increase the variety in the training data: vertical flips, and rotations of 0, 90, 180, and 270 degrees are randomly applied to incoming patches. The model performance is measured with the overall accuracy, the average class accuracy, and the kappa score.

The architectures of the BNN and the CNN networks are identical and detailed in Tab. I. It consists of three convolutional blocks and one fully connected layer. The convolutional blocks consist of a convolutional layer, followed by an activation function, followed by layer normalization. The activation function within the CNN blocks in the CNN is ReLU and in the BNN is Softplus. The receptive field size in the three convolutional layers is  $3 \times 3$ . The number of filters in these three layers are 128, 256, and 512. The fully connected layer has 4068 nodes. In the last layer, the activation function is Log Softmax. To simulate the limited training data situation, 20 pixels per class have been chosen as the training set. Since there are multiple possibilities of selecting training set, we perform the experiments 20 times and report the mean and standard deviation of the performance metrics.

BNN inference is done by drawing 50 samples, which can be seen as an ensemble of 50 networks. For comparison, we also report in the first experiment results for performing only a single BNN draw, denoted as “Bayesian NN (single draw)”.

The first experiment investigates the classification performance and studies the robustness to overfitting. The second experiment investigates the performances when progressively pruning model weights. The third experiment illustrates the uncertainty metric by the BNN and its reliability.

### C. Experiment I: Classification Results

Table II reports classification results for all comparison methods. The BNN performs better than the CNN for all datasets and outperforms the Random Forest. For the Botswana and Pavia datasets, BNN mean Kappa score outperforms the CNN by 0.032 and 0.025 units. CNN and BNN perform comparably on the Salinas dataset. Additionally, the BNN achieves a lower variance of the scores in the Botswana and Pavia datasets, which implies a more stable performance across the test runs. Performing only a single network draw achieves already a reasonably good performance for the BNN. However, ensemble learning with 50 sample networks further improves the performance. A detailed investigation of the class-based

TABLE II: Comparison of classification performance between random forests, standard CNN, and the proposed Bayesian NN with a single inference step and 50 inference steps.

Model	Kappa Score	Overall Acc.
<b>Pavia Dataset</b>		
Random Forest	$0.7730 \pm 0.0535$	$83.64 \pm 4.02$
CNN	$0.8849 \pm 0.0300$	$91.84 \pm 3.00$
Bayesian NN (single draw)	$0.8943 \pm 0.0220$	$92.52 \pm 1.65$
Bayesian NN	$0.9034 \pm 0.0185$	$93.19 \pm 1.29$
<b>Botswana Dataset</b>		
Random Forest	$0.8376 \pm 0.0277$	$85.02 \pm 2.55$
CNN	$0.8987 \pm 0.0164$	$90.65 \pm 1.52$
Bayesian NN (single draw)	$0.9315 \pm 0.0128$	$93.68 \pm 1.18$
Bayesian NN	$0.9383 \pm 0.0137$	$94.31 \pm 1.26$
<b>Salinas Dataset</b>		
Random Forest	$0.7481 \pm 0.0318$	$77.23 \pm 2.94$
CNN	$0.7857 \pm 0.0197$	$80.82 \pm 1.74$
Bayesian NN (single draw)	$0.7870 \pm 0.0278$	$80.77 \pm 2.46$
Bayesian NN	$0.7886 \pm 0.0277$	$80.92 \pm 2.48$

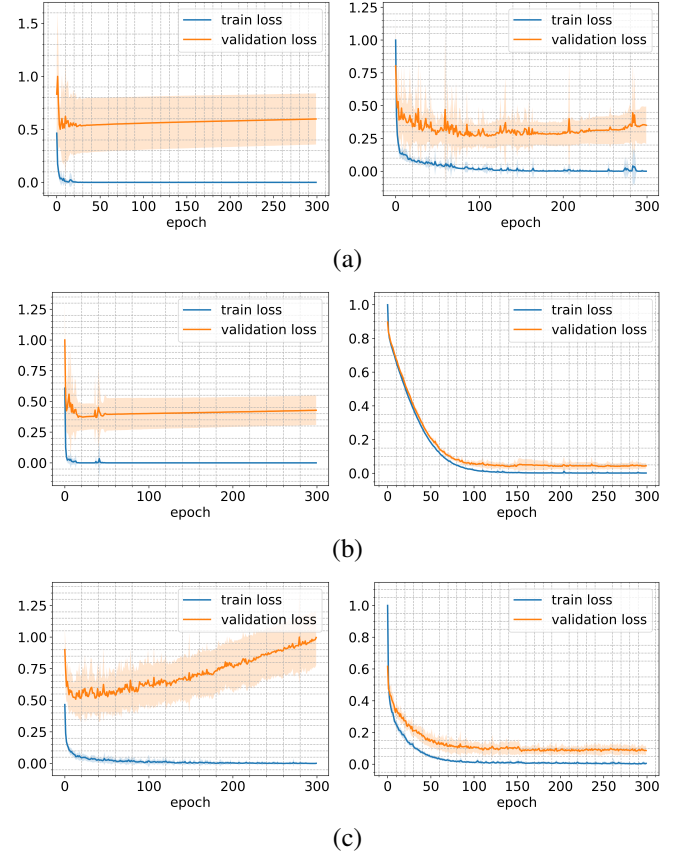


Fig. 3: Train and validation loss of CNN (left) and Bayesian NN (right) on (a) Pavia Centre, (b) Botswana, and (c) Salinas datasets.

models’ prediction results are provided in the supplementary materials, in Tab. III, IV, and V.

Studying the evolution of the train and validation loss during training may reveal indicators for network overfitting. Figure 3 shows the losses for the CNN on the left and the BNN on the right on the Pavia Centre, Botswana, and Salinas datasets. The plot lines show the means and standard deviations of the loss

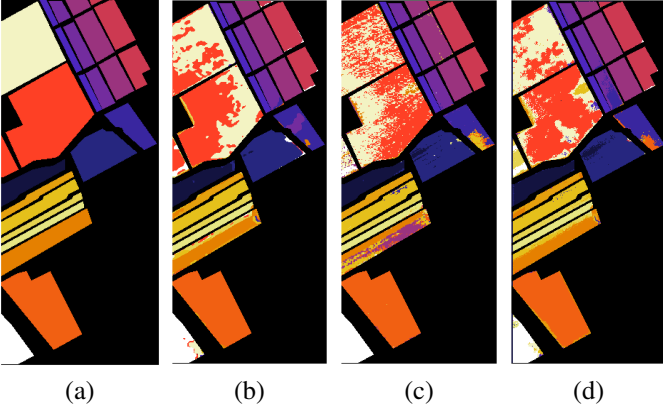


Fig. 4: Prediction of trained Bayesian networks on Salinas dataset. (a) Ground-truth, (b) CNN (c) Random Forest, (d) Bayesian (BNN) predictions.

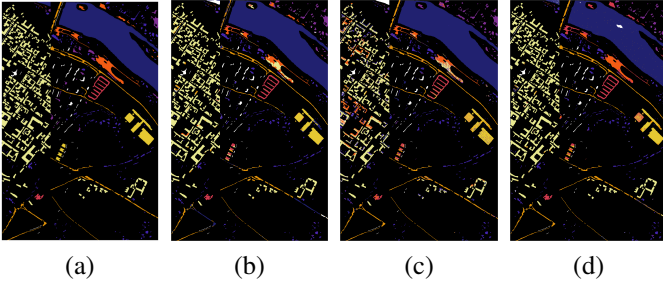


Fig. 5: Prediction of trained Bayesian networks on Pavia dataset. (a) Ground-truth, (b) CNN (c) Random Forest, (d) Bayesian (BNN) predictions.

values over all experiments. In all cases, the Bayesian model exhibits a more desirable behavior. In the Salinas dataset, after around 20 epochs, the CNN validation loss starts to increase while the training loss keeps decreasing. This indicates the network cannot generalize anymore and is already overfitting, whereas the Bayesian model validation loss keeps decreasing or remains almost constant, even until epoch 300. This indicates that the BNN is less prone to overfitting. Similar behavior can be observed for the Botswana dataset. The loss curves for the Pavia dataset are quite comparable for the BNN and CNN models.

Qualitative results on the Pavia and Salinas datasets are shown in Fig. 4 and Fig. 5. Analogously to the results in Tab. II, the Bayesian architecture outperforms the CNN model. This can be particularly well be observed in the large homogeneous areas of the Salinas dataset.

#### D. Experiment II: Robustness against Pruning

This pruning experiment is performed on the models that were trained for Experiment I. We iteratively prune 10% of the available network weights. More in detail, CNN pruning is performed by pruning the weights with the smallest magnitude (absolute value). BNN pruning is performed by pruning the weights with the highest probability of being zero. This process is done for all the experiments, and the mean and the standard

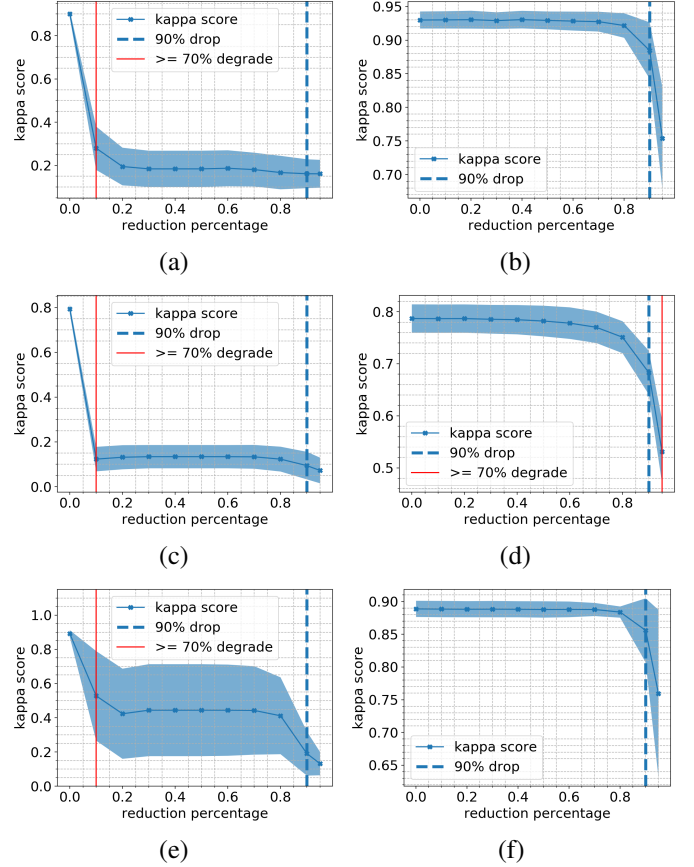


Fig. 6: Kappa score after global pruning of the networks. The left column shows the CNN and the right column shows the BNN. (a) and (b) are computed on Botswana, (c) and (d) on Salinas, and (e) and (f) on the Pavia dataset.

deviation of the kappa scores are provided in Fig. 6. In this figure, the red line indicates where the model reaches below 70% of its initial kappa score, and the blue dashed line indicates where 90% of the weights have been filtered.

The results are similar across all three datasets. The CNN performance deteriorates relatively quickly. The 70% performance degradation is reached when pruning only 10% of the weights. On the other hand, the kappa score of the BNNs remains high when even large numbers of parameters are pruned. Even after pruning 90% of the network weights, the kappa score is still above 70%. Hence, we conclude that the Bayesian network is more stable, and it can be reduced to a much smaller sub-network. Hence, the Bayesian CNN can maintain the high performance under higher compression ratios and has a higher compression capability.

#### E. Experiment III: Evaluation of Uncertainties

One of the advantages of Bayesian networks over the non-Bayesian networks is the additional uncertainty metric. As discussed in section III, there are two types of uncertainties: one accounts for uncertainty in the model prediction, and the other one accounts for the uncertainty caused by the data. In this section, since we want to observe the uncertainty in the input data, we will use the *Aleatoric* uncertainty.

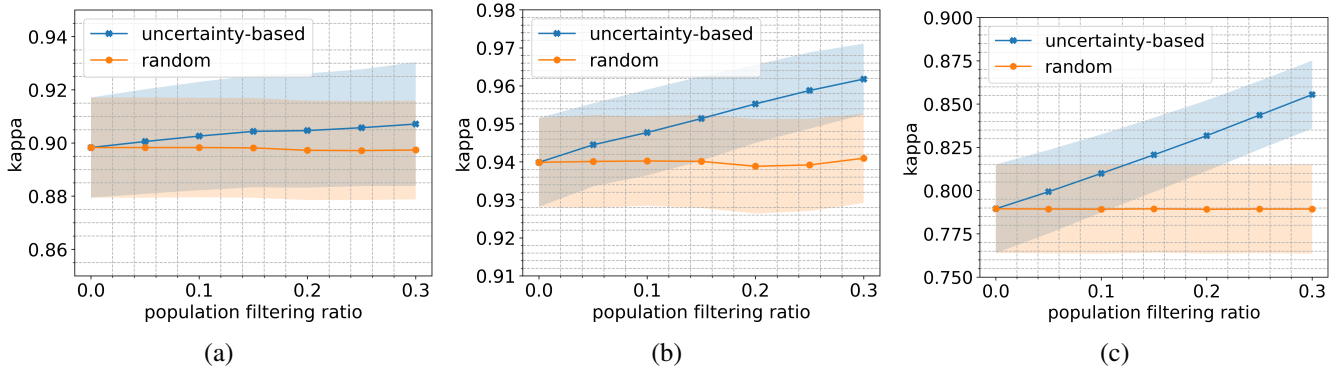


Fig. 7: Kappa score versus uncertain data filtering on (a) Pavia, (b) Botswana, and (c) Salinas datasets. Filtering out the uncertain test samples improves the classification performance, which indicates that the uncertainty has a positive correlation with the prediction error.

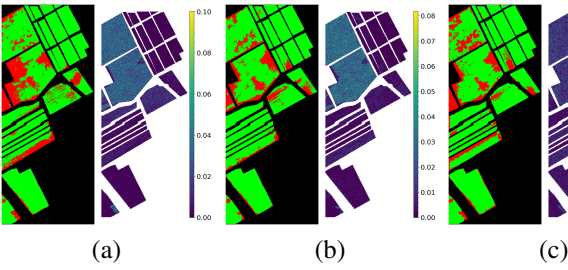


Fig. 8: Prediction correctness (left) versus the uncertainty (right) for three Bayesian networks trained on Salinas dataset.

We design the following experiment to examine whether the uncertainty provided by the network is informative and correlates with the data quality. The quality of the uncertainty metric is assessed by removing a part of the test data. In one variant, we remove just a random portion of the test data. In a second variant, we remove the most uncertain test data points. These dataset reduction approaches are put in relation to the prediction accuracy for the Pavia Centre and Salinas datasets to visually observe the effectiveness of the uncertainty metric.

Figure 7 shows the results. For all datasets, filtering up to 30% of the uncertain test data points results in a significant improvement in the kappa scores. This indicates that the BNN uncertainty can serve as a predictor for samples that are likely misclassified.

Figure 8 qualitatively shows on the Salinas dataset how the uncertainty metric can indicate the prediction reliability. Three trained Bayesian networks are used to visualize the uncertainty. The outputs of these networks are shown in the subfigures (a), (b), and (c). Each subfigure consists of a left part and a right part. The left part shows in green correctly labeled pixels, and in red wrongly labeled pixels. The right part indicates the associated uncertainty. It can be observed that the areas of wrong prediction exhibit by tendency also higher uncertainty.

## VI. CONCLUSION

This paper investigated the Bayesian convolutional neural network for HSRS image classification with severely limited

training data and compared it with a similar frequentist CNN and an off-the-shelf Random Forest. Bayesian methods, in theory, are more robust against overfitting, especially in the case of limited data. The experimental results in this work demonstrated that a Bayesian network outperforms a similar frequentist CNN and Random Forest. Furthermore, the loss plots illustrate that the Bayesian CNN is, for all datasets, more robust against overfitting compared to the non-Bayesian CNN. Moreover, through a set of pruning and re-validation experiments, the Bayesian network has been shown to converge to a considerably smaller and more compact sub-network. This makes them more suitable to be used on devices with less memory, e.g., embedded chips and FPGAs.

In another aspect, the uncertainty provided by the Bayesian network has been studied. It has been observed that the *Aleatoric* uncertainty has a direct correlation with the prediction error: Filtering out uncertain test data enhances the model's performance on the remainder of the test set, whereas randomly filtering the test data does not have any impact on the model's performance. It indicates that the uncertainty metric correlates with the prediction error, and depending on the application, it can be used to enhance the model's prediction.

## REFERENCES

- [1] S. Valero, P. Salembier, and J. Chanussot, "Hyperspectral image representation and processing with binary partition trees," *IEEE Transactions on Image Processing*, vol. 22, no. 4, pp. 1430–1443, 2013.
- [2] C.-I. Chang, *Hyperspectral Imaging: Techniques for Spectral Detection and Classification*. Plenum Publishing Co., 2003.
- [3] G. Hughes, "On the mean accuracy of statistical pattern recognizers," *IEEE Transactions on Information Theory*, vol. 14, no. 1, pp. 55–63, 1968.
- [4] A. Davari, H. C. Özkan, A. Maier, and C. Riess, "Fast and efficient limited data hyperspectral remote sensing image classification via gmm-based synthetic samples," *IEEE Journal of Selected Topics in Applied Earth Observations and Remote Sensing*, vol. 12, no. 7, pp. 2107–2120, 2019.
- [5] A. Davari, E. Aptoula, B. Yanikoglu, A. Maier, and C. Riess, "Gmm-based synthetic samples for classification of hyperspectral images with limited training data," *IEEE Geoscience and Remote Sensing Letters*, vol. 15, no. 6, pp. 942–946, 2018.
- [6] M. Chi, R. Feng, and L. Bruzzone, "Classification of hyperspectral remote-sensing data with primal svm for small-sized training dataset problem," *Advances in Space Research*, vol. 41, no. 11, pp. 1793–1799, 2008.



- [7] Q. Jackson and D. A. Landgrebe, "An adaptive classifier design for high-dimensional data analysis with a limited training data set," *IEEE Transactions on Geoscience and Remote Sensing*, vol. 39, no. 12, pp. 2664–2679, 2001.
- [8] J. Xia, J. Chanussot, P. Du, and X. He, "Rotation-based support vector machine ensemble in classification of hyperspectral data with limited training samples," *IEEE Transactions on Geoscience and Remote Sensing*, vol. 54, no. 3, pp. 1519–1531, 2016.
- [9] A. A. Davari, E. Aptoula, and B. Yanikoglu, "On the effect of synthetic morphological feature vectors on hyperspectral image classification performance," in *2015 23rd Signal Processing and Communications Applications Conference (SIU)*, pp. 653–656, IEEE, 2015.
- [10] X. Kang, X. Xiang, S. Li, and J. A. Benediktsson, "Pca-based edge-preserving features for hyperspectral image classification," *IEEE Transactions on Geoscience and Remote Sensing*, vol. 55, no. 12, pp. 7140–7151, 2017.
- [11] M. Dalla Mura, J. A. Benediktsson, B. Waske, and L. Bruzzone, "Morphological attribute profiles for the analysis of very high resolution images," *IEEE Transactions on Geoscience and Remote Sensing*, vol. 48, no. 10, pp. 3747–3762, 2010.
- [12] I. J. Goodfellow, J. Pouget-Abadie, M. Mirza, B. Xu, D. Warde-Farley, S. Ozair, A. Courville, and Y. Bengio, "Generative adversarial networks," 2014.
- [13] A. Shrivastava, T. Pfister, O. Tuzel, J. Susskind, W. Wang, and R. Webb, "Learning from simulated and unsupervised images through adversarial training," in *Proceedings of the IEEE conference on computer vision and pattern recognition*, pp. 2107–2116, 2017.
- [14] R. Dietrich-Sussner, A. Davari, T. Schehaus, M. Braun, V. Christlein, A. Maier, and C. Riess, "Synthetic glacier sar image generation from arbitrary masks using pix2pix algorithm," in *2021 IEEE International Geoscience and Remote Sensing Symposium IGARSS*, pp. 4548–4551, IEEE, 2021.
- [15] L. He, J. Li, C. Liu, and S. Li, "Recent advances on spectral–spatial hyperspectral image classification: An overview and new guidelines," *IEEE Transactions on Geoscience and Remote Sensing*, vol. 56, no. 3, pp. 1579–1597, 2018.
- [16] P. Ghamisi, E. Maggiori, S. Li, R. Souza, Y. Tarabla, G. Moser, A. De Giorgi, L. Fang, Y. Chen, M. Chi, S. B. Serpico, and J. A. Benediktsson, "New frontiers in spectral-spatial hyperspectral image classification: The latest advances based on mathematical morphology, markov random fields, segmentation, sparse representation, and deep learning," *IEEE Geoscience and Remote Sensing Magazine*, vol. 6, no. 3, pp. 10–43, 2018.
- [17] Y. Chen, Z. Lin, X. Zhao, G. Wang, and Y. Gu, "Deep learning-based classification of hyperspectral data," *IEEE Journal of Selected topics in applied earth observations and remote sensing*, vol. 7, no. 6, pp. 2094–2107, 2014.
- [18] K. Makantasis, K. Karantzalos, A. Doulamis, and N. Doulamis, "Deep supervised learning for hyperspectral data classification through convolutional neural networks," in *2015 IEEE International Geoscience and Remote Sensing Symposium (IGARSS)*, pp. 4959–4962, 2015.
- [19] A. Ben Hamida, A. Benoit, P. Lambert, and C. Ben-Amar, "DEEP LEARNING APPROACH FOR REMOTE SENSING IMAGE ANALYSIS," in *Big Data from Space (BiDS'16)* (S. P. M. P. Giorgio, ed.), (Santa Cruz de Tenerife, Spain), p. 133, Publications Office of the European Union, Mar. 2016.
- [20] Y. Luo, J. Zou, C. Yao, X. Zhao, T. Li, and G. Bai, "Hsi-cnn: A novel convolution neural network for hyperspectral image," in *2018 International Conference on Audio, Language and Image Processing (ICALIP)*, pp. 464–469, 2018.
- [21] N. Audebert, B. L. Saux, and S. Lefèvre, "Deep learning for classification of hyperspectral data: A comparative review," *CoRR*, vol. abs/1904.10674, 2019.
- [22] Y. Chen, L. Zhu, P. Ghamisi, X. Jia, G. Li, and L. Tang, "Hyperspectral images classification with gabor filtering and convolutional neural network," *IEEE Geoscience and Remote Sensing Letters*, vol. 14, no. 12, pp. 2355–2359, 2017.
- [23] E. Aptoula, M. C. Ozdemir, and B. Yanikoglu, "Deep learning with attribute profiles for hyperspectral image classification," *IEEE Geoscience and Remote Sensing Letters*, vol. 13, no. 12, pp. 1970–1974, 2016.
- [24] W. Li, C. Chen, M. Zhang, H. Li, and Q. Du, "Data augmentation for hyperspectral image classification with deep cnn," *IEEE Geoscience and Remote Sensing Letters*, vol. 16, no. 4, pp. 593–597, 2018.
- [25] X. He and Y. Chen, "Transferring cnn ensemble for hyperspectral image classification," *IEEE Geoscience and Remote Sensing Letters*, vol. 18, no. 5, pp. 876–880, 2020.
- [26] X. Cao, J. Yao, Z. Xu, and D. Meng, "Hyperspectral image classification with convolutional neural network and active learning," *IEEE Transactions on Geoscience and Remote Sensing*, vol. 58, no. 7, pp. 4604–4616, 2020.
- [27] W. L. Buntine and A. Weigend, "Bayesian back-propagation," *Complex Syst.*, vol. 5, 1991.
- [28] C. Blundell, J. Cornebise, K. Kavukcuoglu, and D. Wierstra, "Weight uncertainty in neural networks," 2015.
- [29] J. Denker and Y. Lecun, "Transforming neural-net output levels to probability distributions," in *Advances in Neural Information Processing Systems (NIPS 1990)*, Denver, CO, April 1991 (R. Lippmann, J. Moody, and D. Touretzky, eds.), vol. 3, Morgan Kaufmann, 1991.
- [30] N. Srivastava, G. Hinton, A. Krizhevsky, I. Sutskever, and R. Salakhutdinov, "Dropout: A simple way to prevent neural networks from overfitting," *Journal of Machine Learning Research*, vol. 15, no. 56, pp. 1929–1958, 2014.
- [31] S. Wang and C. Manning, "Fast dropout training," in *Proceedings of the 30th International Conference on Machine Learning* (S. Dasgupta and D. McAllester, eds.), vol. 28 of *Proceedings of Machine Learning Research*, (Atlanta, Georgia, USA), pp. 118–126, PMLR, 17–19 Jun 2013.
- [32] Y. Gal and Z. Ghahramani, "Bayesian convolutional neural networks with bernoulli approximate variational inference," 2016.
- [33] A. Graves, "Practical variational inference for neural networks," in *NIPS*, 2011.
- [34] K. Shridhar, F. Laumann, and M. Liwicki, "Uncertainty estimations by softplus normalization in bayesian convolutional neural networks with variational inference," 2019.
- [35] Y. Lecun, L. Bottou, Y. Bengio, and P. Haffner, "Gradient-based learning applied to document recognition," *Proceedings of the IEEE*, vol. 86, no. 11, pp. 2278–2324, 1998.
- [36] K. Shridhar, F. Laumann, and M. Liwicki, "A comprehensive guide to bayesian convolutional neural network with variational inference," 2019.
- [37] S. Kullback and R. A. Leibler, "On information and sufficiency," *Ann. Math. Statist.*, vol. 22, no. 1, pp. 79–86, 1951.
- [38] D. P. Kingma, T. Salimans, and M. Welling, "Variational dropout and the local reparameterization trick," 2015.
- [39] A. Der Kiureghian and O. Ditlevsen, "Aleatory or epistemic? does it matter?," *Structural Safety*, vol. 31, pp. 105–112, 03 2009.
- [40] M. Dalla Mura, J. Atli Benediktsson, B. Waske, and L. Bruzzone, "Extended profiles with morphological attribute filters for the analysis of hyperspectral data," *International Journal of Remote Sensing*, vol. 31, no. 22, pp. 5975–5991, 2010.
- [41] L. Breiman, "Random forests," *Machine Learning*, vol. 45, no. 1, pp. 5–32, 2001.

# Supplementary material for "Bayesian Convolutional Neural Networks for Limited Data Hyperspectral Remote Sensing Image Classification"

Mohammad Joshaghani, Amirabbas Davari, Faezeh Nejati Hatamian, Andreas Maier, Christian Riess

## VII. CLASS-WISE PERFORMANCE

The class-wise performance of the Bayesian CNN classifiers on the Botswana, Pavia Centre, and Salinas datasets are presented in Tab. III, Tab. IV, and Tab. V, respectively.

TABLE III: Bayesian network's class-wise accuracy on Botswana dataset.

Name	Train/Test	RF	CNN	BNN
Water	20/105	100.00 $\pm$ 0.00	99.88 $\pm$ 0.29	99.52 $\pm$ 1.09
Hippo grass	20/41	88.66 $\pm$ 3.39	97.07 $\pm$ 5.15	98.78 $\pm$ 3.32
Floodplain grasses1	20/96	94.87 $\pm$ 3.94	92.67 $\pm$ 5.53	96.98 $\pm$ 3.15
Floodplain grasses2	20/78	81.58 $\pm$ 6.67	88.93 $\pm$ 4.95	92.14 $\pm$ 9.37
Reeds1	20/105	76.36 $\pm$ 4.99	80.68 $\pm$ 7.40	89.08 $\pm$ 7.87
Riparian	20/105	63.00 $\pm$ 10.36	76.72 $\pm$ 7.86	73.48 $\pm$ 10.62
Firescare2	20/100	97.83 $\pm$ 1.10	97.25 $\pm$ 4.54	98.54 $\pm$ 3.79
Island interior	20/72	100.00 $\pm$ 0.00	85.00 $\pm$ 14.03	96.41 $\pm$ 7.69
Acacia woodlands	20/127	90.65 $\pm$ 9.11	88.23 $\pm$ 8.23	93.95 $\pm$ 6.32
Acacia shrublands	20/94	73.03 $\pm$ 12.38	98.07 $\pm$ 4.01	95.83 $\pm$ 5.20
Acacia grasslands	20/123	69.44 $\pm$ 14.83	85.28 $\pm$ 8.06	93.85 $\pm$ 4.79
Short mopane	20/61	93.95 $\pm$ 2.31	98.77 $\pm$ 1.70	98.09 $\pm$ 2.36
Mixed mopane	20/104	90.44 $\pm$ 7.07	99.19 $\pm$ 1.65	97.86 $\pm$ 3.28
Exposed soils	20/38	70.53 $\pm$ 8.91	85.53 $\pm$ 4.67	91.58 $\pm$ 6.09
Kappa		0.8376 $\pm$ 0.0277	0.8987 $\pm$ 0.0164	0.9315 $\pm$ 0.0128
Overall Accuracy		85.02 $\pm$ 2.55	90.65 $\pm$ 1.52	93.68 $\pm$ 1.18
Average Accuracy		79.36 $\pm$ 5.67	90.95 $\pm$ 5.58	94.01 $\pm$ 5.35

TABLE IV: Bayesian network's class-wise accuracy on Pavia dataset.

Name	Train/Test	RF	CNN	BNN
Water	20/32976	98.98 $\pm$ 0.19	99.65 $\pm$ 0.36	99.10 $\pm$ 1.10
Trees	20/3789	66.27 $\pm$ 7.08	76.00 $\pm$ 6.83	74.88 $\pm$ 6.70
Asphalt	20/1535	32.73 $\pm$ 2.05	36.93 $\pm$ 8.77	34.48 $\pm$ 4.24
Self-Blocking Bricks	20/1333	79.02 $\pm$ 8.70	92.00 $\pm$ 12.48	92.80 $\pm$ 5.25
Bitumen	20/3282	49.98 $\pm$ 10.80	71.56 $\pm$ 17.79	65.61 $\pm$ 12.44
Tiles	20/4614	91.52 $\pm$ 5.50	91.19 $\pm$ 6.07	86.63 $\pm$ 8.03
Shadows	20/3634	74.78 $\pm$ 7.55	72.68 $\pm$ 10.77	80.02 $\pm$ 6.72
Meadows	20/21403	73.69 $\pm$ 12.63	92.67 $\pm$ 5.68	94.44 $\pm$ 4.57
Bare Soil	20/1422	93.87 $\pm$ 2.06	97.67 $\pm$ 2.47	92.74 $\pm$ 7.51
Kappa		0.7730 $\pm$ 0.0535	0.8849 $\pm$ 0.0300	0.8943 $\pm$ 0.0220
Overall Accuracy		83.64 $\pm$ 4.02	91.84 $\pm$ 3.00	92.52 $\pm$ 1.65
Average Accuracy		66.08 $\pm$ 5.65	90.95 $\pm$ 5.58	94.01 $\pm$ 5.35

TABLE V: Bayesian network's class-wise accuracy on Salinas dataset.

Name	Train/Test	RF	CNN	BNN
Broccoli green weeds 1	20/975	97.36 $\pm$ 2.53	96.21 $\pm$ 3.25	86.37 $\pm$ 22.95
Broccoli green weeds 2	20/1853	92.90 $\pm$ 5.91	90.75 $\pm$ 7.51	90.00 $\pm$ 5.90
Fallow	20/958	57.88 $\pm$ 21.66	73.51 $\pm$ 17.83	71.55 $\pm$ 12.02
Fallow rough plow	20/667	99.59 $\pm$ 0.23	98.05 $\pm$ 1.59	99.00 $\pm$ 0.51
Fallow smooth	20/1309	94.74 $\pm$ 4.49	88.75 $\pm$ 7.41	87.68 $\pm$ 6.46
Stubble	20/1950	97.47 $\pm$ 1.75	99.90 $\pm$ 0.28	99.64 $\pm$ 0.83
Celery	20/1760	99.99 $\pm$ 0.03	98.69 $\pm$ 1.69	99.08 $\pm$ 0.80
Grapes untrained	20/5606	49.79 $\pm$ 19.51	58.32 $\pm$ 12.70	60.75 $\pm$ 11.42
Soil vineyard develop	20/3072	94.20 $\pm$ 5.03	95.65 $\pm$ 3.32	96.12 $\pm$ 2.38
Corn green weeds	20/1609	53.97 $\pm$ 17.86	54.29 $\pm$ 16.34	59.85 $\pm$ 18.65
Lettuce romaine 4wk	20/504	92.71 $\pm$ 3.36	86.74 $\pm$ 8.00	88.95 $\pm$ 7.38
Lettuce romaine 5wk	20/934	89.17 $\pm$ 15.41	97.61 $\pm$ 4.78	96.73 $\pm$ 3.24
Lettuce romaine 6wk	20/428	96.37 $\pm$ 3.51	97.06 $\pm$ 3.48	96.08 $\pm$ 5.33
Lettuce romaine 7wk	20/525	85.74 $\pm$ 9.66	95.04 $\pm$ 4.51	95.63 $\pm$ 3.65
Vineyard untrained	20/3604	63.42 $\pm$ 19.78	70.65 $\pm$ 17.38	67.17 $\pm$ 17.80
Vineyard vertical trellis	20/874	99.32 $\pm$ 1.41	85.01 $\pm$ 9.24	91.33 $\pm$ 6.02
Kappa		0.7481 $\pm$ 0.0318	0.7857 $\pm$ 0.0197	0.7870 $\pm$ 0.0278
Overall Accuracy		77.23 $\pm$ 2.94	80.82 $\pm$ 1.74	80.77 $\pm$ 2.46
Average Accuracy		80.27 $\pm$ 7.77	86.64 $\pm$ 7.46	86.62 $\pm$ 7.83

## VIII. IMPACT OF THE TRAIN SPLIT

The training data has been selected as a connected component (CC) around a random pixel instead of randomly picking pixels throughout the image. This way, we minimize the chance of overlap between the training set, and the validation and test sets. To illustrate the difference caused by the random and CC sampling strategies and visualize how much the overlap decreases using the CC sampling policy, we carried out a random train split and a CC split. Then, the histogram of the distance of all pixels in the validation and test sets from the closest training point of the same class is measured and plotted in 9 as an accumulative bar plot. The plot compares the widely used random pixel sampling (top) to the connected-component training split used in this work (bottom). Plots (a), (b), (c) operate on the Botswana, Pavia, and Salinas datasets. On the  $x$ -axis, the distance between training and test pixels is shown. On the  $y$ -axis, the cumulative relative frequencies are shown that a training pixel is within  $x$  pixels next to a test pixel. We use the patch size of  $9 \times 9$  pixels in the neural networks. Hence, we highlight the overlap percentage at the distance of 9 pixels. If the distance of the patch centers is below 9 pixels, an overlap occurs with at least one training patch from the same class. The less these occurrences happen, the more realistic the validation results would be.

As we can see in Fig. 9, the difference of the overlap between the two methods is quite large; in the Salinas dataset, using random train data extraction, more than 72% of the validation

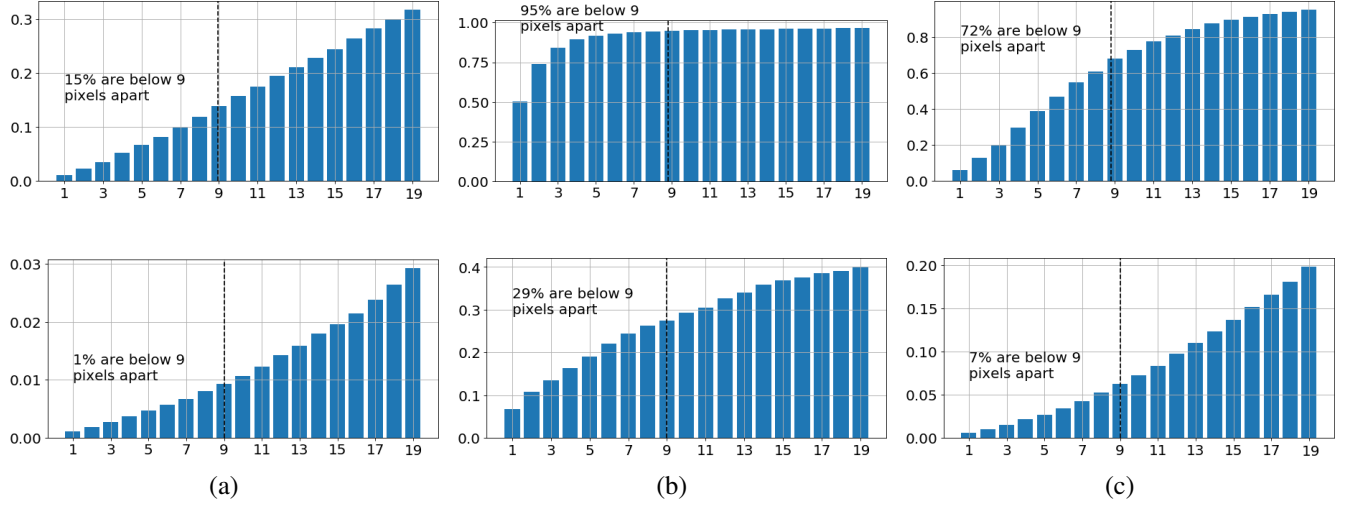


Fig. 9: Random (upper) and Connected-Component (lower) train split method comparison for (a) Pavia, (b) Botswana, and (c) Salinas datasets.

and test data are less than 9 pixels apart and are at least partly fed into the network during training. On the other hand, this number is around 7% in the case of connected component sampling method. For the Botswana dataset, a random split partially feeds at least 95% of the validation and test patches into the network during training, whereas 29% is fed when using connected component training data. The same story applies to the Pavia dataset, and the overlap rate is more than 15% in random split, as opposed to 1% on the other method. These numbers suggest that using the connected component method would result in a more realistic measure of the model's generalization capability.